Reversal in Thermally Driven Rotation of Chiral Liquid Crystal Droplets

Shunsuke Takano,[1, *] Takuya Nakanishi,[2] Kenta Nakagawa,[2] and Toru Asahi[1, 2, †]

[1]*Graduate School of Science and Engineering, Waseda University,*
TWIns, 2-2 Wakamatsu-cho, Shinjuku, Tokyo, 162-8480, Japan
[2]*Comprehensive Research Organization, Waseda University, TWIns, 2-2 Wakamatsu-cho, Shinjuku, Tokyo, 162-8480, Japan*
(Dated: 24 April 2024)

For chiral liquid crystals that express topologically protected defects and thermally driven mechanical rotation, the size- and temperature-driven reversal of the rotational direction of their droplets was demonstrated even under a fixed temperature gradient. This unconventional reversal indicates the dependence of thermomechanical coupling on the molecular orientational order, this dependence is justified through an examination of the size, temperature, and molecular structure as well as by phenomenological arguments on the order parameter.

Chirality is an abundant frontier for the emergence of topological structures and transport dynamics in condensed matter. In liquid crystals (LCs), chirality allows a pseudoscalar (Lifshitz invariant) $\mathbf{n} \cdot \nabla \times \mathbf{n} = n_i \epsilon_{ijk} \nabla_j n_k$ $(i, j, k = 1, 2, 3)$ to be nonzero [1, 2], where $\mathbf{n}$ is the director, a locally defined unit vector along which LC molecules tend to orient. The pseudoscalar stabilizes a spontaneous helical director field, similar to Dzyaloshinsky-Moriya interaction in magnets [3, 4]. The helical field is utilized for displays, thermometers, and asymmetric reactions for helical polymerization [5, 6].

When chiral nematic (N^*) LCs are confined in a spherical droplet, the periodic layers of the helical director field deform into concentric shells under degenerate planar anchoring (Fig. 1). Through these concentrically layered shells, a line-like topological defect stretches from the center to the surface of the droplet due to geometrical frustration prohibiting the director from continuously covering the entire sphere. The defect has a winding number (or the topological charge) of $+2$, equal to the Euler characteristic of the sphere [7]. This orientational structure is known as the radial spherical structure (RSS) and displays distinct textures, namely concentric circles with a radial line and a double spiral [see Figs. 1(a) and (b), respectively] [8–12]. Within the defect, the molecular orientational order is more violated than in the surroundings, but the loss of free energy is restricted, thus providing a net stabilization of the system. Some models of the director field have been proposed to suppress the reduction of the order in the defect [13, 14]. Skyrmions, vortex-like structures formed in blue phases [15, 16] and in confined spaces [17], have been noted to contribute to the stabilization of the defect [12]. Also, in defects appearing as vortices in superfluid and in Type II superconductors, the amplitude of the order parameter (OP) representing the density of Bose-Einstein condensates decreases and usually reaches zero [18, 19]. The vortices in superfluid ^{4}He capturing solid nanoparticles have been optically visualized [20], and superconductors permit the magnetic field to penetrate only through the latticed vortices [21, 22]. In LCs, defects are considered to be analogues to Dirac magnetic monopoles [7]
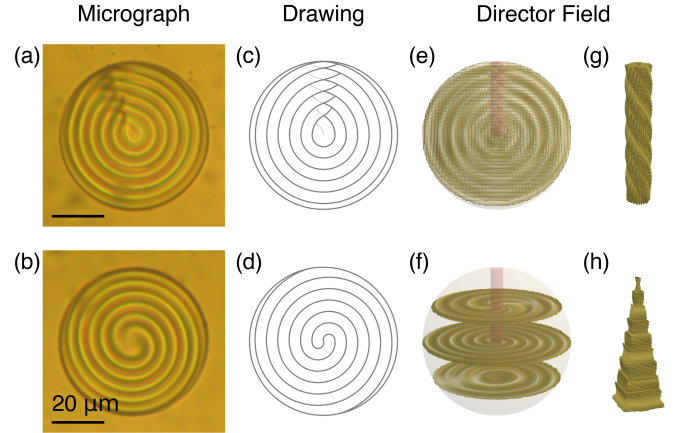

Micrograph | Drawing | Director Field

FIG. 1. RSS is distinct orientational structure composed of concentrically layered shells and a single radial topological defect line (filament). (a) and (b) Micrographs of spherical droplets of N^* LCs in glycerol, which were taken in absence of temperature gradients by detaching chamber from temperature controllers. (c) and (d) Drawings of textures when observed from two different orthogonal angles. (e)–(h) Director field under Ansatz that constrains director at droplet surface to tangent plane, derived in Ref. [11]. Directors are visualized as cylinders. Red region represents filament. (e) Concentric director field near plane where filament lies. (f) Spiral director field on sections orthogonal to filament. (g) Cylindrical region around the filament. (h) Pyramid region opposite filament across center of the droplet. Helical director field forms layers with their normal along radial axis.

and cosmic strings [23].

The chirality of LCs induces their dynamical rotation under temperature gradients [24–35]. This rotation is attributed to the coupling between translation and rotation by the helical director field [32] or the conversion of thermal energy into torque by thermomechanical (thermohydrodynamic) coupling [25, 33, 36]. Thermomechanical coupling is characterized by a pseudoscalar coupling constant ν, which is nonzero if and only if the LC is locally chiral. Recently, the role of topology has been discussed for rotations caused by the coupling of translation and rotation [31, 35] or by chemomechanical (chemohydrody-

namic) coupling [37]. Nevertheless, topological involvement in thermomechanical coupling is still unclear due to the experimental difficulties.

Here, we investigate the role of topological defects in thermomechanical coupling by focusing on RSS. Hereinafter, we refer to the defect as a filament to remind the reader of its finite thickness. A recently developed method [34] enables weak thermomechanical coupling to be detected.

Experimental system.—N^* LC mixtures nCB(X) were prepared by mixing nematic LCs 4′-alkyl-4-cyanobiphenyls nCB (n = 5, 6, 7), with chiral dopants (X)-2-octyl 4-[4-(hexyloxy)benzoyloxy]benzoate (X = R, S) at a concentration of approximately 1.5% w/w. nCB(X) was dispersed as spherical droplets with a non-uniform radius in immiscible glycerol, where Marangoni convection and mass diffusion fluxes are effectively suppressed [31, 32], and then introduced into a glass chamber. A temperature gradient was applied to the nCB(X) droplets vertically upward (defined as the z-axis) by heating the top and cooling the bottom of the chamber, and Rayleigh-Bénard convection, in which heated fluid floats [38, 39], was prevented. Details on the methods are available in the Supplemental Material [40].

Reversal with radius.—Figure 2(a) shows the rotational motion of 7CB(R) droplets under a steady temperature gradient. As the clean chamber prevented the cyanobipheyl LCs from adhering to the walls, the rotational motion of the LC droplets was successfully demonstrated [40]. Remarkably, the rotational direction of the droplets reversed depending on their radii. Figure 2(c) shows the temporal change in the rotational angle of a large droplet α (with radius of 13.0 μm) and a small droplet β (with radius of 9.1 μm). Droplets α and β rotated in the opposite directions due to the difference in their radii. As conventionally known, inverting the chirality of sample or the direction of the temperature gradient causes the reversal of rotational direction [26, 34, 56]. However, the present reversal with size (droplet radius) was not predicted and is presented in this Letter for the first time.

The reversal of the rotational direction is attributed to the reversal of torque exerting on the droplet. A droplet with RSS comprises two orientational structures (Fig. 1): concentric shells consisting of the periodic layers of a helical director field and the radial filament of a topological defect [7], each of which has a different dimension in terms of extensive property.

Figure 3(a) schematically shows the dimension of these structures in RSS. The shells and the filament are three- and quasi-one-dimensional with the volume increasing in proportion to the cubic radius R^3 and to the radius R^1, respectively. Thermomechanical torques must occur in opposite directions between them; torques in nCB(R) are induced anticlockwise and clockwise in the shells and the filament, respectively. The torques proportional to
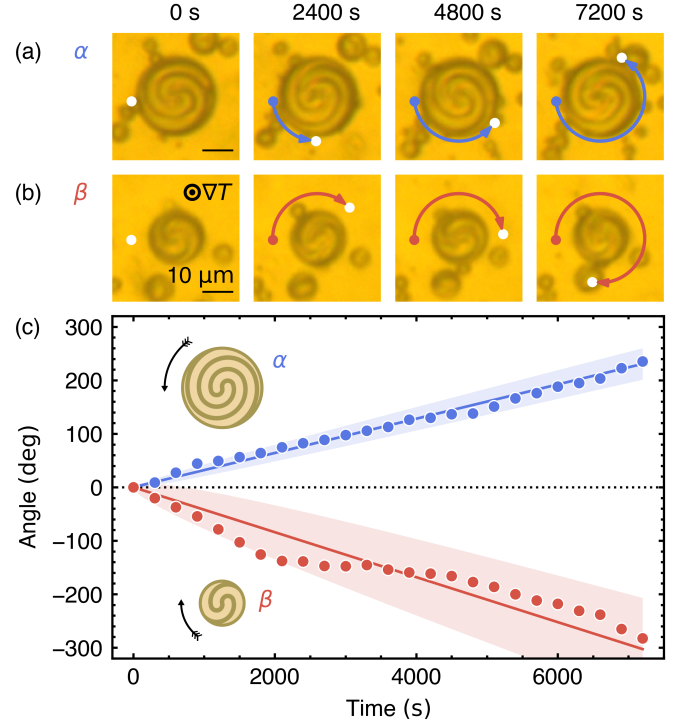

FIG. 2. Rotation of droplets. (a) and (b) Micrographs of rotating droplets of different sizes, α and β, under temperature gradient $\nabla_z T = +1.00 \times 10^4 \, \mathrm{K\,m^{-1}}$ (target symbol in (b) is perpendicular to this figure in the direction of the reader). Filament is oriented parallel to optical axis. Initial and current directions of droplets are represented by colored and white circles, respectively. See also Supplemental Material, Movie S4 [40]. (c) Rotation angle of droplets α (blue) and β (red) against time. Positive in angle axis represents anticlockwise rotation. Measured rotation angles from initial position are plotted with regression lines. Shaded areas indicate uncertainties of doubled standard deviations due to thermal fluctuations. For smaller droplets, violation of angle was more significant due to thermal fluctuations. The contrast of the images was adjusted.

each volume compete with each other inside the droplet, and the sum of conflicting torques determines the rotational direction of the droplet. A droplet with a radius large enough, in which the shells are volumetrically dominant, experiences a net anticlockwise torque, whereas a droplet whose radius is so small that the filament transcends the shells experiences a net clockwise torque. Note that, heat is converted into torque differently depending on the microscopic orientational order of the molecules in each structure.

The torque competition between these two types of structures in the droplets is formulated by the dimensional analysis below. A minimal expression of the dissipation function Φ up to numerical factors is a quadratic form of the variables of angular velocity ω_0 and temper-
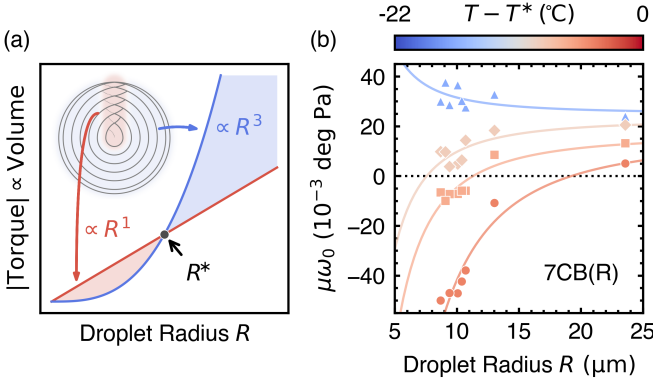
FIG. 3. (a) Schematic diagram of torque in constituent structures. Blue and red lines represent torque induced in shells (shaded in blue) and filament (shaded in red), respectively. Each torque is proportional to volume and opposite to each other. Rotational direction of droplets shifts at switching radius R^* where torques are in equilibrium. (b) Angular velocity against radius. Angular velocity ω_0 is scaled by viscosity of glycerol μ. Plots are measured values and curves are regression lines obeying $\mu\omega_0 = a_3 - a_1 R^{-2}$, complementing Eq. (2) with temperature-dependent factors a_3 and a_1. Color of each plot and curve indicates the temperature and corresponds to color bar above.

ature gradient $\nabla_z T$, as

$$\Phi = -2\nu \left(R^3 - q_0^{-2} R^1 \right) \omega_0 \nabla_z T + \mu R^3 \omega_0^2 + \kappa T^{-1} R^3 (\nabla_z T)^2. \tag{1}$$

The first term represents the energy converted per unit time through thermomechanical coupling. The coefficients with dimensions of volume R^3 and $q_0^{-2} R^1$ describe the contributions of the three-dimensional shells and the quasi-one-dimensional filament, respectively. Adopting Onsager's variational principle [57], we obtain the angular velocity in the steady state,

$$\omega_0(R) = \left(1 - \frac{1}{(q_0 R)^2} \right) \frac{\nu \nabla_z T}{\mu}, \tag{2}$$

which minimizes the dissipation function in Eq. (1) under a fixed temperature gradient $\nabla_z T$. The contribution of the filament, represented by the factor $(q_0 R)^{-2}$, is responsible for the radial dependence and reversal of the droplets' rotation. Eq. (2) derives a switching radius R^* that is almost equal to the period of the helical director field $|q_0|^{-1} \simeq 10\,\mu m$. As shown in Fig. 3(b), Eq. (2) describes the dependence of the angular velocity on the radius with the reversal of the rotational direction well.

Molecular order.—In the analysis above, we assumed that the molecular order leads to a difference in the direction of the induced torque [Fig. 3(a)], which is natural because thermomechanical coupling would relate to certain intermolecular correlations as an analogy to viscosity [5]. The intermolecular correlation is represented by the director **n** and the scalar OP S, where the latter is the height of molecular order and reaches zero in isotropic (I)
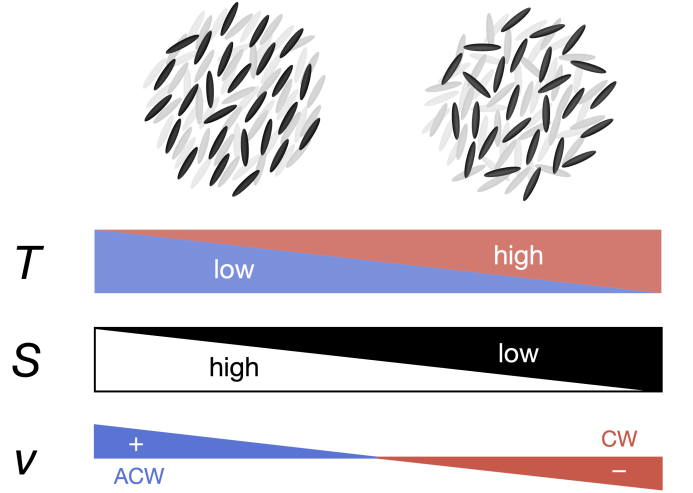

FIG. 4. Dependence of coupling constant ν on scalar OP S and temperature T. (left to right) Gradation from highly ordered state (high S, low T) with positive ν and torque of anticlockwise (ACW) rotation to poorly ordered state (low S, high T) with negative ν and torque of clockwise (CW) rotation.

phase. The significance of S in physical properties of LCs is widely recognized. In particular, the variation of S explains the temperature dependence of birefringence [58], the elastic constants [48, 59], and Leslie viscosity coefficients [52].

Figure 4 schematically shows the relationship between S and the coupling constant ν. In nCB(R), ν becomes positive and negative when S is high and low, respectively. Since S is reduced in the filament similar to the amplitudes of the macroscopic wavefunction at vortices of superconductors, ν is negative in the filament and, in contrast, positive in the shells with higher S. In nCB(S), the mirrored counterpart, ν has the opposite sign.

Reversal with temperature.—As temperature rises, S declines due to thermal fluctuation, and ν changes accordingly; thus, the reversal of the rotational direction with temperature is also expected (Fig. 4). Figures 5(a)–(d) show the rotational direction of droplets at different temperatures, clearly demonstrating the abovementioned reversal. For instance, droplets of 7CB(R) with a radius of approximately $10\,\mu m$ rotated anticlockwise at $33.1°C$ but clockwise at temperatures above $35.5°C$ [Fig. 5(a)]. The switching radius R^* observed near $10\,\mu m$ coincides with the dimensional analysis in Eq. (2). The shift of R^* with temperature indicates that the coupling constant ν tends to be negative due to the decrease in S at high temperatures and, in contrast, at a sufficiently low temperature, all droplets rotate anticlockwise since ν is positive thanks to the higher molecular order even in the filament. The spiral texture (namely, period and sense of helix) was identical at high and low temperatures. This is consistent with the independence
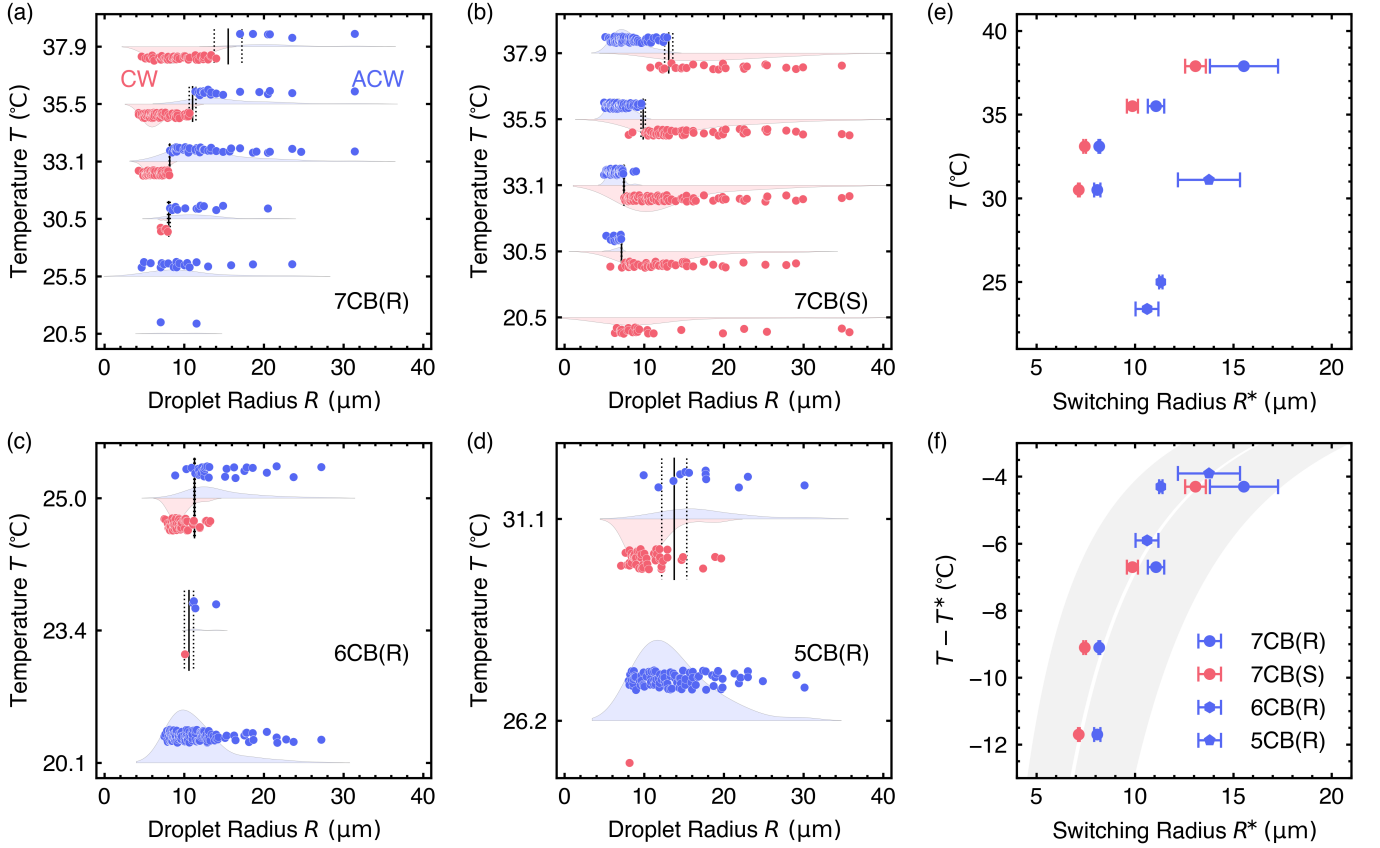
FIG. 5. (a)–(d) Temperature dependence of rotational direction of droplets of 7CB(R), 7CB(S), 6CB(R), and 5CB(R). All of them showed reversal of rotational direction with temperature. Anticlockwise (ACW) and clockwise (CW) rotations are plotted in blue and red, respectively. Shaded areas indicate violin plots, showing the frequency distribution of radius across rotational direction and temperature determined by kernel density estimation. Since temperature is treated as a categorical variable, its original scaling is not displayed. Black solid and dotted lines show switching radius R^* and its confidence interval with doubled standard deviations, respectively. (e) and (f) Switching radius against temperature T and relative temperature $T - T^*$, respectively. Error bars indicate confidence interval as shown in (a)–(d).

of the helical field and thermomechanical coupling [27].

This reversal with temperature was also confirmed in 7CB(S). Droplets with a radius of approximately $10\,\mu\mathrm{m}$ rotated clockwise and anticlockwise at $33.1°\mathrm{C}$ and above $35.5°\mathrm{C}$, respectively [Fig. 5(b)]. The rotational direction at a given temperature and radius was opposite for 7CB(R) and 7CB(S). Similar reversal of the rotational direction was observed for all the alkyl chain lengths considered, including $n = 5$ and 6 [Figs. 5(c) and (d)].

Figures 5(e) and (f) show the switching radius against the temperature. The temperature dependence of R^* varied for every alkyl chain length n [Fig. 5(e)]. Notably, however, a common dependence was found among n on the relative temperature $T - T^*$, where T^* is the N^*-I transition temperature, indicating that the reversal with temperature was driven by S (rather than T itself).

A theoretical insight.—We recast the theory of thermomechanical coupling conventionally formulated with the director $\mathbf{n}$. Omitting the contributions of the electromagnetic field, hydrodynamic flow and elastic distortion,

the evolution of the director, which is purely driven by thermomechanical coupling, is [36]

$$\dot{n}_i = -\nu\epsilon_{ijk}n_j\nabla_k T, \qquad (3)$$

where ν is the coupling constant renormalized by division by the viscosity against the background flow. The director $\mathbf{n}$ specifies only the mean orientation direction of the molecules, and $\mathbf{n}$ ignores the degree of molecular orientation, which is represented by the scalar OP S. The complete OP for describing the microscopic molecular order is a second-order symmetric traceless tensor (the Q-tensor)

$$Q_{ij} = \frac{3}{2}S\left(n_i n_j - \frac{1}{3}\delta_{ij}\right), \qquad (4)$$

whose non-degenerate eigenvalue is equal to S and its eigenvector is $\mathbf{n}$ [48]. The evolution of the orientational order is re-described by replacing $\mathbf{n}$ with Q. Consistent with the existing theory shown in Eq. (3), assume that

the evolution of Q is proportional to the temperature gradient ∇T:

$$\dot{Q}_{ij} = -L_{ijk}\nabla_k T, \qquad (5)$$

where L_{ijk} is a third-order tensor coefficient being invariant with respect to $i \leftrightarrow j$, inheriting the symmetry of $\dot{Q}_{ij}$. Since L has the same symmetry as the N^* phase, it must be a function of Q. Since elastic distortion [48] and anisotropic viscosity [52] are successfully described by tensorial arguments, an analogy of them, L is expanded by terms of the powers of Q [40]. These considerations on the symmetry derive the S-dependent coupling constant

$$\nu(S) = \nu_1 + \nu_2 S, \qquad (6)$$

where ν_1 and ν_2 are pseudoscalars hardly varying with temperature. Eq. (6) indicates that the strength and the direction of thermomechanical torque are influenced by the molecular order parametrized by S. As reported for chiral ferroelectric LCs, spontaneous polarization reverses its direction with temperature because of a shift in molecular order, especially conformation [60, 61]. Thus, the sign reversal of ν is probably induced by changes in molecular order due to temperature or frustrations. Though the sign reversal of ν indicates the opposites signs between ν_1 and ν_2, its necessity is not derived within the present phenomenological argument. Instead, molecular simulations [62] or statistical mechanics would be valid for estimating ν_1 and ν_2. The present reconstruction adopting Q, a suitable OP for expressing the microscopic molecular orientational order, will support the future elucidation of the molecular mechanisms of thermomechanical coupling.

Conclusion.—We have found that droplets of chiral LCs with topological defects show reversal of rotational motion under a temperature gradient. This nontrivial reversal depending on size and temperature has not yet been expected but is ascribed to the dependence of thermomechanical coupling on the degree of molecular orientational order, which is justified by our phenomenological argument. In the context of topology of materials, the phase or direction components of the order parameter is usually taken up [63]. We propose, however, that the amplitude component is also noteworthy for emergence of distinct properties. Future studies will explore superconductors and magnets, as well as LCs, for analogous behaviors.

* shunsuke.t-8395@akane.waseda.jp
† tasahi@waseda.jp

[1] P. G. de Gennes, Short range order effects in the isotropic phase of nematics and cholesterics, Mol. Cryst. Liq. Cryst. **12**, 193 (1971).
[2] A. Bogdanov, On the stability of localized states in nonlinear field models with Lifshitz invariants, Sov. Phys. JETP Lett. **68**, 317 (1998).
[3] I. Dzyaloshinsky, A thermodynamic theory of "weak" ferromagnetism of antiferromagnetics, Journal of Physics and Chemistry of Solids **4**, 241 (1958).
[4] T. Moriya, Anisotropic superexchange interaction and weak ferromagnetism, Phys. Rev. **120**, 91 (1960).
[5] P. G. de Gennes and J. Prost, *The Physics of Liquid Crystals*, 2nd ed. (Oxford University Press, Oxford, New York, 1995).
[6] K. Akagi, G. Piao, S. Kaneko, K. Sakamaki, H. Shirakawa, and M. Kyotani, Helical polyacetylene synthesized with a chiral nematic reaction field, Science **282**, 1683 (1998).
[7] M. V. Kurik and O. D. Lavrentovich, Topological defects of cholesteric liquid crystals for volumes with spherical shape, Mol. Cryst. Liq. Cryst. **72**, 239 (1982).
[8] O. Lehmann, Tropfen und Säulen kristallinischer Flüssigkeiten mit verdrehter Struktur, Ann. Phys. (Leipzig) **357**, 736 (1917).
[9] C. Robinson, J. C. Ward, and R. B. Beevers, Liquid crystalline structure in polypeptide solutions. part 2, Discuss. Faraday Soc. **25**, 29 (1958).
[10] Y. Bouligand and F. Livolant, The organization of cholesteric spherulites, J. Phys. France **45**, 1899 (1984).
[11] J. Bezić and S. Žumer, Structures of the cholesteric liquid crystal droplets with parallel surface anchoring, Liq. Cryst. **11**, 593 (1992).
[12] D. Seč, T. Porenta, M. Ravnik, and S. Žumer, Geometrical frustration of chiral ordering in cholesteric droplets, Soft Matter **8**, 11982 (2012).
[13] F. Xu and P. P. Crooker, Chiral nematic droplets with parallel surface anchoring, Phys. Rev. E **56**, 6853 (1997).
[14] A. Darmon, M. Benzaquen, D. Seč, S. Čopar, O. Dauchot, and T. Lopez-Leon, Waltzing route toward double-helix formation in cholesteric shells, Proc. Natl. Acad. Sci. U.S.A. **113**, 9469 (2016).
[15] D. C. Wright and N. D. Mermin, Crystalline liquids: the Blue Phases, Rev. Mod. Phys. **61**, 385 (1989).
[16] J. Pišljar, S. Ghosh, S. Turlapati, N. V. S. Rao, M. Škarabot, A. Mertelj, A. Petelin, A. Nych, M. Marinčič, A. Pusovnik, M. Ravnik, and I. Muševič, Blue Phase III: Topological fluid of skyrmions, Phys. Rev. X **12**, 011003 (2022).
[17] J. V. Selinger, Interpretation of saddle-splay and the Oseen-Frank free energy in liquid crystals, Liq. Cryst. Rev. **6**, 129 (2018).
[18] A. A. Abrikosov, Dokl. Akad. Nauk SSSR **86**, 489 (1952).
[19] V. L. Ginzburg and L. P. Pitaevskii, On the theory of superfluidity, Sov. Phys. JETP **34**, 1240 (1958).
[20] G. Bewley, D. Lathrop, and K. Sreenivasan, Visualization of quantized vortices, Nature **441** (2006).
[21] A. A. Abrikosov, Sov. Phys. JETP **5**, 1174 (1957).
[22] D. Cribier, B. Jacrot, L. M. Rao, and B. Farnoux, Mise en évidence par diffraction de neutrons d'une structure

periodique du champ magnetique dans le niobium supra-conducteur, Phys. Lett. **9**, 106 (1964).

[23] C. Meng, J.-S. Wu, and I. I. Smalyukh, Topological steering of light by nematic vortices and analogy to cosmic strings, Nat. Mater. **22**, 64 (2023).

[24] O. Lehmann, Structur, System und magnetisches Verhalten flüssiger Krystalle und deren Mischbarkeit mit festen, Ann. Phys. (Leipzig) **307**, 649 (1900).

[25] N. Éber and I. Jánossy, An experiment on the thermomechanical coupling in cholesterics, Mol. Cryst. Liq. Cryst. **72**, 233 (1982).

[26] P. Oswald and A. Dequidt, Measurement of the continuous Lehmann rotation of cholesteric droplets subjected to a temperature gradient, Phys. Rev. Lett. **100**, 217802 (2008).

[27] P. Oswald, Microscopic vs. macroscopic origin of the Lehmann effect in cholesteric liquid crystals, Eur. Phys. J. E **35**, 10 (2012).

[28] J. Yoshioka, F. Ito, Y. Suzuki, H. Takahashi, H. Takizawa, and Y. Tabe, Director/barycentric rotation in cholesteric droplets under temperature gradient, Soft Matter **10**, 5869 (2014).

[29] T. Yamamoto, M. Kuroda, and M. Sano, Three-dimensional analysis of thermo-mechanically rotating cholesteric liquid crystal droplets under a temperature gradient, Eur. Phys. Lett. **109**, 46001 (2015).

[30] S. Bono, Y. Maruyama, and Y. Tabe, Formation and dynamics of the aggregates of cholesteric double-twist cylinders, Soft Matter **14**, 9798 (2018).

[31] J. Yoshioka and F. Araoka, Topology-dependent self-structure mediation and efficient energy conversion in heat-flux-driven rotors of cholesteric droplets, Nat. Commun. **9**, 432 (2018).

[32] P. Oswald, J. Ignés-Mullol, and A. Dequidt, Lehmann rotation of cholesteric droplets driven by Marangoni convection, Soft Matter **15**, 2591 (2019).

[33] P. Oswald, A. Dequidt, and G. Poy, Thermomechanical effects in liquid crystals, in *Liquid Crystals: New Perspectives*, edited by P. Pieranski and M. H. Godinho (John Wiley & Sons, 2021) Chap. 3, pp. 117–191.

[34] S. Takano, S. Bono, and Y. Tabe, Heat-flux-driven rotation of cholesteric droplets dispersed in glycerol, J. Phys. Soc. Jpn. **92**, 024601 (2023), https://doi.org/10.7566/JPSJ.92.024601.

[35] J. Yoshioka, Y. Ito, and K. Fukao, Morphogenesis of a chiral liquid crystalline droplet with topological reconnection and Lehmann rotation, Sci. Rep. **preprint** (2023).

[36] F. M. Leslie, Some thermal effects in cholesteric liquid crystals, Proc. Roy. Soc. A **307**, 359 (1968).

[37] F. Bunel and P. Oswald, Chemical Leslie effect in a chiral smectic-C^* film: Nonsingular target patterns, Phys. Rev. E **107**, 024703 (2023).

[38] H. Bénard, Les tourbillons cellulaires dans une nappe liquide. -méthodes optiques d'observation et d'enregistrement, J. Phys. Theor. Appl. **10**, 254 (1901).

[39] Lord Rayleigh, LIX. On convection currents in a horizontal layer of fluid, when the higher temperature is on the under side, Lond. Edinb. Dublin Philos. Mag. J. Sci. **32**, 529 (1916), https://doi.org/10.1080/14786441608635602.

[40] See Supplemental Material at [url_to_be_inserted] for details on materials, methods and derivations as well as movies, which includes Refs. [41–55].

[41] P. G. de Gennes, An analogy between superconductors and smectics A, Solid State Commun. **10**, 753 (1972).

[42] National Astronomical Observatory of Japan, ed., *Chronological Scientific Tables* (Maruzen, Tokyo, 2011).

[43] S. Pestov and V. Vill, Liquid crystals, in *Springer Handbook of Condensed Matter and Materials Data*, edited by W. Martienssen and H. Warlimont (Springer Berlin Heidelberg, Berlin, Heidelberg, 2005) pp. 941–977.

[44] G. Poy and S. Žumer, Ray-based optical visualisation of complex birefringent structures including energy transport, Soft Matter **15**, 3659 (2019).

[45] E. Buckingham, On physically similar systems; illustrations of the use of dimensional equations, Phys. Rev. **4**, 354 (1914).

[46] C. W. Oseen, The theory of liquid crystals, Trans. Faraday Soc. **29**, 883 (1933).

[47] F. C. Frank, I. liquid crystals On the theory of liquid crystals, Discuss. Faraday Soc. **25**, 19 (1958).

[48] T. C. Lubensky, Molecular description of nematic liquid crystals, Phys. Rev. A **2**, 2497 (1970).

[49] J. L. Ericksen, Conservation laws for liquid crystals, Trans. Soc. Rheol. **5**, 23 (1961).

[50] F. M. Leslie, Some constitutive equations for liquid crystals, Arch. Ration. Mech. Anal. **28**, 265 (1968).

[51] O. Parodi, Stress tensor for a nematic liquid crystal, J. Phys. **31**, 581 (1970).

[52] H. Imura and K. Okano, Temperature dependence of the viscosity coefficients of liquid crystals, Jpn. J. Appl. Phys. **11**, 1440 (1972).

[53] R. S. Porter and J. F. Johnson, The rheology of liquid crystals, in *Rheology: Theory and Applications*, Vol. 4, edited by F. R. Eirich (Academic Press, New York, London, 1967).

[54] C. Gähwiller, The viscosity coefficients of a room-temperature liquid crystal (MBBA), Phys. Lett. A **36**, 311 (1971).

[55] G. Poy and P. Oswald, On the existence of the thermomechanical terms of Akopyan and Zel'dovich in cholesteric liquid crystals, Liq. Cryst. **45**, 1428 (2018), https://doi.org/10.1080/02678292.2018.1446552.

[56] P. Oswald, A. Dequidt, and G. Poy, Lehmann effect in nematic and cholesteric liquid crystals: a review, Liq. Cryst. Rev. **7**, 142 (2019).

[57] L. Onsager, Reciprocal relations in irreversible processes. I., Phys. Rev. **37**, 405 (1931).

[58] J. Li, C.-H. Wen, S. Gauza, R. Lu, and S.-T. Wu, Refractive indices of liquid crystals for display applications, J. Disp. Technol. **1**, 51 (2005).

[59] I. Haller and J. D. Litster, Light scattering spectrum of a nematic liquid, Mol. Cryst. Liq. Cryst. **12**, 277 (1971).

[60] J. W. Goodby, E. Chin, M. Geary, J. S. Patel, and P. L. Finn, The Ferroelectric and Liquid-crystalline Properties of Some Chiral Alkyl 4-n-Alkanoyloxybiphenyl-4'-carboxylates, J. Chem. Soc., Faraday trans. **83**, 3429 (1987).

[61] S. A. Różański, Effect of confinement on polarization sign inversion temperature in ferroelectric liquid crystal, Acta. Phys. Pol. **139**, 417 (2021).

[62] S. Sarman, Y.-L. Wang, and A. Laaksonen, Thermomechanical coupling in coarse grained cholesteric liquid crystal model systems with pitches of realistic length, Phys. Chem. Chem. Phys. **18**, 16822 (2016).

[63] K. Nomura, S. Ryu, A. Furusaki, and N. Nagaosa, Cross-correlated responses of topological superconductors and superfluids, Phys. Rev. Lett. **108**, 026802 (2012).